Check for updates

# Biophysical analysis of gelatin and PLGA nanoparticle interactions with complex biomimetic lung surfactant models†

W. Daear, [ID] ‡ K. Sule, [ID] ‡ P. Lai [ID] § and E. J. Prenner [ID] *

Biocompatible materials are increasingly used for pulmonary drug delivery, and it is essential to understand their potential impact on the respiratory system, notably their effect on lung surfactant, a monolayer of lipids and proteins, responsible for preventing alveolar collapse during breathing cycles. We have developed a complex mimic of lung surfactant composed of eight lipids mixed in ratios reported for native lung surfactant. A synthetic peptide based on surfactant protein B was added to better mimic the biological system. This model was used to evaluate the impact of biocompatible gelatin and poly(lactic-co-glycolic acid) nanoparticles. Surface pressure–area isotherms were used to assess lipid packing, film compressibility and stability, whereas the lateral organization was visualized by Brewster angle microscopy. Nanoparticles increased film fluidity and altered the monolayer collapse pressure. Bright protruding clusters formed in their presence indicate a significant impact on the lateral organization of the surfactant film. Altogether, this work indicates that biocompatible materials considered to be safe for drug delivery still need to be assessed for their potential detrimental impact before use in therapeutic applications

## 1. Introduction

Nanotechnology has applications in various fields of science and technology that involve medicine and biotechnology. As the name implies, materials of interest are on the nanometer scale.[1,2] One of the key goals of nanotechnology applications in terms of drug delivery goes back to the German scientist Paul Ehrlich in the 1890s, who envisioned the creation of a "magic bullet", where medicine can be targeted and delivered to a specific location of choice.[3]

A more recent approach for this concept is the use of nanoparticles (NPs) that are designed to encapsulate, attach, or adsorb drugs and deliver them to a target location.[4] Furthermore, their small size results in a large surface area to volume ratio allowing for higher drug loading per particle.[5] Moreover, this large surface area offers a high capacity for chemical modification or attachment of different ligands. These surface modifications can be used to improve circulation times and aid in targeting specific cell types.

An important aspect in drug delivery NPs is the nature of the material used for the drug carrier. In order to avoid or at least reduce side effects of the carrier system, NPs formulated with biocompatible materials can be readily metabolized in the body. This also allows for controlled drug release.[1]

The NPs can be delivered in the human body through a variety of drug delivery routes. More recently, the pulmonary route, which is delivery through the lungs, has gained significant interest. It is non-invasive and ideally suited to directly target lung diseases. Another main reason for the scientific interest is the large surface area of the lungs of around 43–102 m,[2] depending on the age and size of the individual.[6–8] Furthermore, the close proximity to the vascular system allows for local and systematic drug delivery and avoids metabolic break down in the gastrointestinal tract.[8] Systemic pulmonary delivery requires particles to reach the alveoli found at the terminal end of the respiratory tract.

The human lower respiratory tract is composed of the small bronchioles and the alveoli. The alveoli are the site of gas exchange between the blood and external environment where oxygen is taken up, and carbon dioxide is released. The thin alveolar barrier of around 200–500 nm[9,10] is composed of three layers (Fig. S1†). The layer in contact with the blood circulation is composed of type I and type II epithelial pneumocytes. Above the epithelial cells is an aqueous layer of 50–80 nm thick containing macrophages that act as a defense mechanism by eliminating foreign substances.[6,11] In humans, around 300 million alveoli comprise about 95% of the lung's surface area. Both the large surface area and proximity and extent of vascularization are major advantages of this drug delivery route.[12–14]

*Department of Biological Sciences, University of Calgary, Calgary, AB, T2N 1N4, Canada. E-mail: eprenner@ucalgary.ca*

† Electronic supplementary information (ESI) available. See https://doi.org/10.1039/d2ra02859j

‡ Both contributed equally and are listed in alphabetical order.

§ Current address: Rane Pharmaceutical, Edmonton, AB, Canada.

For the NP to pass from the air into circulation it must first come into contact with the lung surfactant. This single molecular layer composed of 90% lipids and 10% protein resides on top of the aqueous layer.

The major role of this monolayer is to reduce the surface tension at the air–water interface, maintain surfactant film stability during exhalation, and aid respreading of the film during inhalation (Fig. S1†). This helps prevent lung collapse during breathing cycles.[15–17] The major lipid classes found in the human lung surfactant include about 70% zwitterionic phosphatidylcholines and about 10% anionic phosphatidylglycerol of the total lipidic components.[18–20] Among the phosphatidylcholines, the saturated dipalmitoylphosphatidylcholine (DPPC) makes up around 50% of the total lipid composition while the rest are the unsaturated form.[18] Interestingly, the phase transition temperature of DPPC is 41 °C[21] above the physiological temperature, which helps to understand its important role to ensure the stability of lung surfactant upon compression during exhalation.[20] In contrast, the fast area increase upon inhalation requires fluid lipids that promote film respreading. This fluidity is provided by unsaturated lipids, such as palmitoyl-oleoylphosphatidylglycerol (POPG)[22] representing a class of negatively charged lipid components. Furthermore, lung surfactant contains about 10% neutral lipids such as cholesterol.[18]

In addition to lipids, lung surfactant also contains about 10% surfactant proteins (SPs), which are present as SP-A, SP-B, SP-C, and SP-D.[16,20] SP-B and SP-C are both hydrophobic whose functions are to aid the lipidic component of the lung surfactant in reducing the surface tension and allow respreading of the monolayer during breathing cycles.[23–25] Controlled and reversible folding of the monolayer to generate multilayer stacks and reverting back to a monolayer is facilitated by the hydrophobic surfactant proteins.[26] While the hydrophilic SP-A and SP-D are involved in the immune response against pathogens.[27–29]

In pulmonary drug delivery, it is crucial that inhaled nanoparticles have minimal impact on lung surfactant function to maintain the ability of surfactant to lower surface tension and to avoid detrimental impacts on respiratory function.

Lung surfactant contains a complex mixture of lipids with varying degrees of acyl chain length and saturation. Many groups have worked on LS model systems based on single lipids like DPPC.[2,3,26,30] We have spent significant efforts to establish a complex biomimetic system[31,32] and complex lung surfactant model systems have also been used in the literature.[26,30,31] In an effort to even better capture the detailed lipid composition, we used custom synthesized 16 : 0/16 : 1 PC and PG, which make up 20% of the total lipid component of the lung surfactant[4] but have not been characterized. The culmination of this work is presented with 7 phospholipids and cholesterol in ratios based on literature reports.[33–36] The stepwise addition of specific lipids to increasingly complex models, allow to assess specific contributions to the overall observed effects.

Another level of complexity is achieved by including surfactant proteins or protein derived peptides. SP-B is required for monolayer to multilayer transition of surfactant important for

function[37,38] but a synthetic SP-B construct (SP-B$_{1–25}$) has been shown to perform similar functions as the full SP-B.[39,40] Thus, this synthetic SP-B fragment was added to our most complex biomimetic model investigated here. To our knowledge, there is no comparable well-defined synthetic model. This system could be used as a tool for *in vitro* screening of different nanomaterials.

This complex lipid–peptide based LS model was used to evaluate the potential impact of two biocompatible materials on surfactant film function in terms of film stability and lateral domain organization by using monolayers at the air–water interface and Brewster angle microscopy. The first is gelatin, a natural polymer obtained from gelatin which has been investigated by our group before.[32,41] The second is a synthetic polymer poly(lactic-co-glycolic) acid (PLGA), which has been used in medical devices and would healing applications.[42–44]

This approach aims to better understand and compare the impact of nanomaterials and their potential to impair surfactant function. As more nanomaterials are designed for drug delivery, these formulations will need to be evaluated. This *in vitro* method provides a tool to screen new nanomaterials before conducting *in vivo* studies.

## 2. Materials and methods

### 2.1. Materials

All lipids were purchased from or custom synthesized 16 : 0/16 : 1-PC (16-1-PC) and 16 : 0/16 : 1-PG(16 : 1-PG) by Avanti Polar Lipids Inc. (Alabaster, AL, USA). Gelatin (type B, bloom of 225), poly(D,L-lactide-co-glycolide) (75 : 25), ethyl acetate, and glutaraldehyde (25% v/v) were purchased from Sigma-Aldrich (Oakville, ON, CA). SP-B$_{1–25}$ peptide, which has a molecular weight of 2.9 kDa, was custom synthesized by AAPPTec (Kentucky, USA) to a 97.5% purity (HPLC) with the following truncated sequence:

NH$_2$-FPIPLPYCWLCRALIKRIQAMIPKG-COOH

These are the first 25 amino acids from the full SP-B protein sequence.[40] SP-B is 79 amino acids long, but the first 25 amino acids was chosen for this work due to their role in the insertion to the lung surfactant monofilm. Acetone, methanol, hexane, and chloroform with an ACS grade were purchased from Fisher Scientific (Ontario, CA). Pluronic F-68 was a donation from collaborators at the University of Alberta (Dr Löbenberg, Faculty of Pharmacy).

### 2.2. Methods

**2.2.1. Gelatin nanoparticle synthesis.** Gelatin NPs (GNPs) were synthesized using an optimized two-step desolvation method.[32,45] 1.25 g of gelatin type B were dissolved in 25 mL of deionized water in an Erlenmeyer flask. The solution was heated to 40 °C on a hot plate before 21 mL of acetone were added dropwise under stirring at 600 rpm in order to precipitate high molecular weight gelatin. The supernatant was discarded and another 25 mL of deionized water were added. The pH was adjusted to 2.5 by using hydrochloric acid. 75 mL of acetone were added dropwise for NP formation until the solution turned

cloudy with an optical density of 0.08 at 600 nm. Subsequently, 250 μL of glutaraldehyde were added to crosslink and stabilize the NPs. The solution was then stirred for 16 hours before excess acetone was removed using a rotary evaporator. The NP solution was stored at 4 °C.

**2.2.2. PLGA nanoparticle synthesis.** PLGA NPs were synthesized using the emulsification-diffusion method.[47] 100 mg of PLGA were dissolved in 10 mL of ethyl acetate constituting the organic phase. For the aqueous phase, 1% (w/v) Pluronic F68 stabilizer was added into 20 mL of ddH$_2$O. The organic phase was combined with the aqueous phase and emulsified by using a probe sonicator (QSonica LLC, USA) at 10 W for 1 min before 80 mL of ddH$_2$O were added under stirring at 600 rpm. The resultant NPs were stored in water at 4 °C.

**2.2.3 Nanoparticle characterization.** Nanoparticles were measured in a clear polystyrene cuvette from Sarstedt (Nümbrecht, Germany) for size and polydispersity analysis with Malvern Zetasizer Nano-ZS from Malvern Panalytical (Quebec, Canada). Each sample was an average of at least 3 measurements.

For zeta potential measurements, nanoparticles were centrifuged and resuspended in a 10 mM NaCl solution at pH 7. The solution was transferred to a folded capillary cell from Malvern (Quebec, Canada) an electric field of 150 mV was applied to measure the electrophoretic mobility. Each sample was an average of at least 3 measurements.

**2.2.4. Lipid solutions.** The selected lipids under study were dissolved in 6 : 4 v/v chloroform : methanol to a final concentration of 1 mM as can be seen below (Table 1).

SP-B$_{1-25}$ along with lipids were added at a 10% weight ratio of lipids, gelatin at a 10 : 1 lipid : NP weight ratio, and PLGA at both 10 : 1 and 1 : 1 lipid : NP weight ratio in 6 : 4 chloroform : methanol.

**2.2.5. Surface pressure–area isotherms.** With both NPs, a 200 cm² Biolin Scientific Teflon Langmuir trough (Gothenburg, Sweden) was used. PLGA NPs are not stable in organic solvents and had to be added to the aqueous subphase. In contrast, gelatin NPs are stable in organic solvents and were deposited at the air–water interface along with the lipids. Surface pressure was measured using a pressure sensor equipped with a Wilhelmy plate.[46] The trough required 120 mL of deionized water as subphase. Compression of the deposited films was performed at 100 cm² min⁻¹ using Teflon barriers after 10 min in order to allow for organic solvent evaporation.

Experiments were performed under ambient conditions with at least 3 replicates for each system.

**2.2.6. Compression modulus.** The compression modulus ($\beta$) was derived from the pressure–area isotherms using the following equation where $C_s$ is the compressibility, $A$ is the molecular area, and $\pi$ is the surface pressure.

$$\beta = \frac{1}{C_s} = -\frac{1}{A} \times \frac{dA}{d\pi} \qquad (1)$$

The reported compression modulus values describe the phases of the deposited monofilms. Values under 12 mN m⁻¹ correspond to the gas phase, 12 mN m⁻¹ to 100 mN m⁻¹ reflect the liquid-expanded (LE) phase, whereas values above 100 mN m⁻¹ correspond to the liquid condensed (LC) phase.[47,48] This analysis reports on the interfacial packing elasticity of monolayers.

**2.2.7. Brewster angle microscopy.** Brewster angle microscopy (BAM) allows for *in situ* visualization of lipid domains without the use of exogenous fluorescent dyes. This is achieved by directing a laser on an aqueous surface at a specific Brewster angle, which is 53.1° for water. At this angle, no light is reflected of the air–water interface. The spreading of a lipid film changes the refractive index resulting in reflections of the film into the camera. BAM images of the investigated were obtained for lipid controls and in the presence of the NP's. For more information on the background of BAM can be found in the ESI.†

The lung surfactant model systems were deposited as described for the pressure–area isotherms. After a 10 min delay, compression was started until the selected surface pressure and stopped to collect images before compression was resumed. Images were obtained by using an EP3 imaging ellipsometer and corresponding EP3 software (Accurion, Goettingen, Germany). Image analysis in terms of area coverage and domain frequency was performed by using ImageJ (NIH, Bethesda, USA). Each image is representative of at least three separate trials.

## 3. Results and discussion

The increased interest in pulmonary drug delivery also includes the need for a better understanding of the impact of drug delivery systems on lung function. An essential element for proper lung function is the surfactant layer within the alveoli that provides the interface between the air and water layer located in top of the lung endothelial cells.

**Table 1** The various model systems tested with the relative molar ratios used. Each system was made to a final 1 mM concentration. The ratios were derived from animal studies[33–36]

| System | Lipid composition | Molar ratio | Final concentration |
|---|---|---|---|
| PC system | DPPC : POPC : 16-1PC | 5.6 : 1 : 1 | 1 mM |
| PG system | DPPG : POPG : SOPG : 16-1PG | 1 : 6 : 4.4 : 2 | 1 mM |
| 8 Lipid system | DPPC : POPC : DPPG : POPG : SOPG : 16-1PC : 16-1PG + cholesterol | 45 : 8 : 1 : 6 : 4.4 : 8 : 2 +2% w/w cholesterol | 1 mM |

While the size dependent deposition and uptake of nanoparticles is well established,[49] the impact of nanomaterials on lung surfactant is less understood. We have shown previously that gelatin NPs exhibit differential interactions with zwitterionic PCs and negatively charges PGs as the latter showed lateral film reorganization by inducing clusters. Moreover, the effect was stronger for saturated DPPG over monounsaturated POPG.[32]

The present work expands the scope to a more complex biomimetic lung surfactant model comprising 8 lipids and a peptide from SP-B and by comparing two biocompatible materials gelatin and PLGA in the form of NPs.

### 3.1. Nanoparticle characterization

Gelatin NPs had a diameter of 110 nm with a polydispersity index of 0.2 and zeta potential of +17 mV at pH of 7. This indicates that the particles are mostly monodisperse in an aqueous suspension.

PLGA NPs had a diameter of 141 nm with a polydispersity index of 0.13 and zeta potential of −26 mV at pH of 7. This also demonstrates a mostly monodisperse suspension.

### 3.2. Individual lipid systems

#### 3.2.1. Pressure–area isotherms and compression modulus.
Drug delivery through the lungs has many advantages due to its ability to deliver both local and systemic treatments. The effect of gelatin NPs on the lung surfactant has been characterized before by our group on lipid model systems.[31,32] In the current work, a hydrophobic peptide based on SP-B was added to the lung surfactant models since SP-B has been shown to be crucial for proper lung surfactant function.[37,38] Fig. 1 presents surface pressure–area and compression isotherms for the two key PC and PG lipids, DPPC and DPPG upon addition of SP-B$_{1-25}$.

DPPC exhibits a characteristic phase coexistence region of LE and LC phases between 85 and 65 Å$^2$ mol$^{-1}$, which is shifted by the peptide to larger areas between 89 and 69 Å$^2$ mol$^{-1}$. This phase coexistence results in distinct domain formation. Upon compression, the continuous slope of DPPC is replaced by an isotherm exhibiting a shoulder at around 20 mN m$^{-1}$ in the presence of SP-B$_{1-25}$ (Fig. 1A, purple arrow) and another inflection at 42 mN m$^{-1}$ to a gentler slope, which is indicative of a film that can withstand compression. This may be due to the formation of functional multilayers, which are important
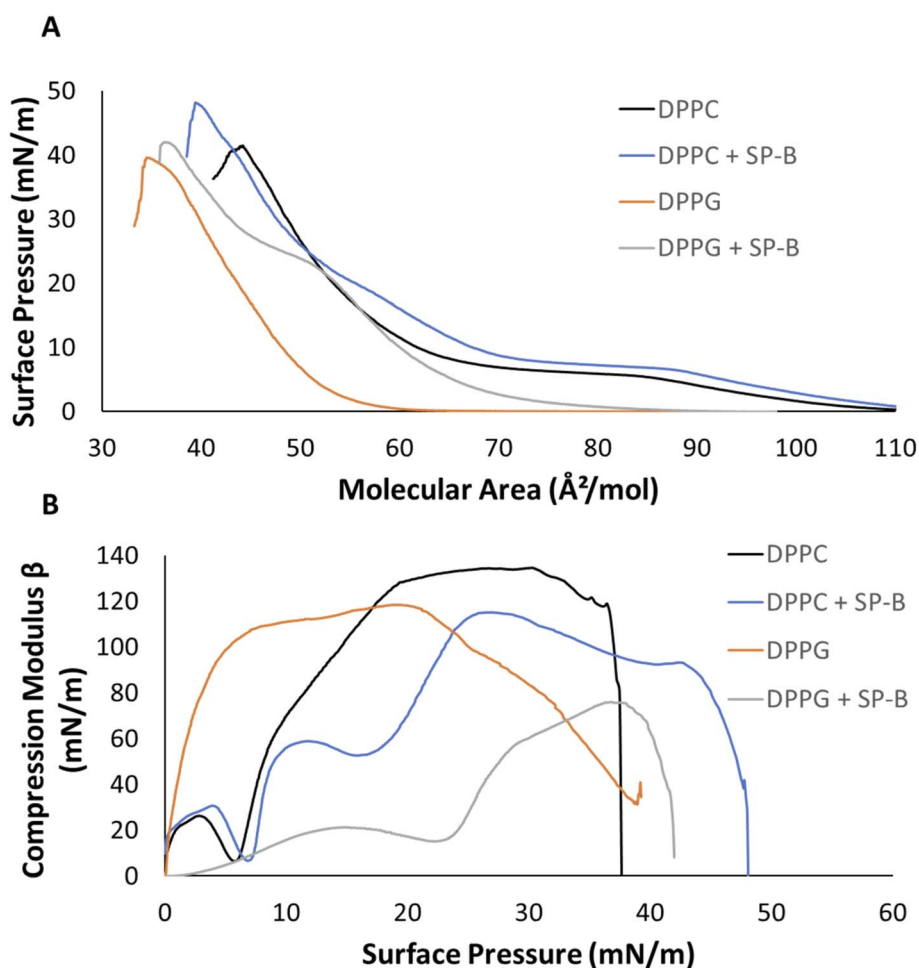


Fig. 1 Pressure–area and compression modulus isotherms of individual lipid systems on an aqueous subphase. (A) Pressure–area isotherm and (B) compression modulus of DPPC, DPPG, and in the presence of SP-B$_{1-25}$ at a 10% weight ratio, respectively. All isotherms collected are an average of the replicates ($n \geq 3$).

for proper surfactant function[50] (Fig. 1A, purple box). SP-B$_{1-25}$ peptide increased the collapse pressure by about 7 mN m$^{-1}$, such film stabilization has been reported before.[16,51,52]

Fig. 1B shows compression modulus (Cm) data according to eqn (1) representing film elasticity. The dip in the isotherm at 6 mN m$^{-1}$ corresponds to the LE-LC phase coexistence region of DPPC (Fig. 1B). Subsequently, Cm values exceeding 100 mN m$^{-1}$ indicated the more rigid LC phase with a maximum of 134.3 mN m$^{-1}$ (Fig. 1B). The addition of 10% by weight SP-B$_{1-25}$ shifted the LE-LC phase coexistence dip to a higher surface pressure of around 8 mN m$^{-1}$ (Fig. 1B). The shoulder around 20 mN m$^{-1}$ in the peptide containing system is highlighted as a dip in the Cm (Fig. 1B). The maximum peak at 115 mN m$^{-1}$ compared to 134.3 mN m$^{-1}$ for controls represents a peptide induced increase in fluidity.

Fig. 1A presents surface pressure–area isotherms for DPPG. The negatively charged phosphatidylglycerol are the second largest lipid class found in human lung surfactant at about 10%.[18,20] DPPG has the same acyl chain composition as DPPC but a smaller glycerol headgroup compared to choline. Both lipids carry a negative charge on the phosphate group, but PC is zwitterionic due to an added positive charge on the quaternary amine. DPPG films lift off at 60 Å$^2$ mol$^{-1}$ and rapidly transitions into the LC phase as seen by the sharp increase in the isotherm slope (Fig. 1A) before collapsing at a surface pressure of 40 mN m$^{-1}$. SP-B$_{1-25}$ caused a significant lift off shift to 89 Å$^2$ mol$^{-1}$, a distinct shoulder at 23 mN m$^{-1}$ and a slight increase in the collapse pressure from 40 to 42 mN m$^{-1}$ (Fig. 1A). The shoulder at 23 mN m$^{-1}$ and shift to smaller molecular areas likely reflects an at least partial squeeze-out of SP-B$_{1-25}$. Collapse pressures for monofilms of protein and peptides have been reported between 15 and 20 mN m$^{-1}$.[53,54]

DPPG entered the LC phase early on during the compression isotherm showing Cm values above 100 mN m$^{-1}$ (Fig. 1B) and with a maximum Cm of 118 mN m$^{-1}$ at a surface pressure of 20 mN m$^{-1}$. The Cm profile for SP-B$_{1-25}$ displayed lower values throughout the entire compression. Once again, the shoulder at 22 mN m$^{-1}$ in the pressure–area isotherm appears as a dip in the Cm graph with a reduced maximum of 76 mN m$^{-1}$. This maximum is also observed at higher surface pressures closer to 38 mN m$^{-1}$ whereas the maximum for DPPG controls appears at much lower pressures (Fig. 1B).

SP-B$_{1-25}$ affected both DPPC and DPPG, and it is known to interact with lung surfactant through electrostatic and hydrophobic interactions, respectively.[55–58] SP-B resides outside of the LC domains, preferentially interacting with the more fluid LS components[59] which are primarily PG lipids. Nevertheless, the rigid sterol cholesterol is also required for proper function of LS[60] and involved in SP-B function.[59] A peptide induced shift to larger areas in the pressure–area isotherms has been observed before for both saturated lipids.[39,61,62] Results from Fig. 1 show that SP-B$_{1-25}$, increased the fluidity of both of DPPC and more so DPPG, as indicated by the lower compression moduli (Fig. 1B).

Hydrophobic SP-B and SP-C are known to facilitate adsorption and spreading of the lung surfactant during breathing cycles through the formation of surface associated LS reservoirs.[63,64] Fig. S2† shows a model to better illustrate the proposed mechanism. This squeeze out effect has been seen previously as well with other systems.[61,65] Lipids are squeezed out during exhalation as the alveolar surface area is reduced by forming multilayer stacks. The further reduction in surface area allows for surfactant to reach near zero surface tensions.[66] SP-B is critical for this function, while SP-C is required for proper function.

### 3.3. Model lipid systems

Analysis of key lipid classes helps to demonstrate the impact of the peptide and illustrates the scope of information obtained from monolayer isotherms. The next step was the analysis of more complex biomimetic systems and their response to NPs made from two biodegradable materials.

**3.3.1. Pressure–area isotherms and compression modulus.** We have previously analyzed DPPC with about 15% POPC.[32] The current model adds a third relevant PC subspecies, a 16 : 0/16 : 1 acyl chained partly unsaturated lipid. The PC lipid mixture was comprised of DPPC, POPC and 16 : 0/16 : 1-PC (16-1-PC) at a molar ratio of 5.6 : 1 : 1, whereby both partly unsaturated lipids exist at an equivalent molar percentage[33] (Fig. 2). POPC is a partly unsaturated lipid found in lung surfactant and carries both a palmitoyl and oleoyl side chains resulting in a phase transition temperature from gel to liquid-crystalline phase of −2 °C.[67] The third lipid in the system, the partly unsaturated 16 : 0/16 : 1 PC (16-1PC) carries palmitoyl and palmitoleoyl side chains. This lipid has a shorter unsaturated acyl chain and had to be custom synthesized by Avantli Polar lipids. There are limited data about its biophysical behavior but one paper using pyrene fluorescence reports a Tm of 30 °C.[68] A Tm in the ∼30 °C seems too high when known melting temperatures for the 18 carbon lipids are considered. Fully saturated DSPC has a Tm of 55 °C, fully unsaturated DOPC has −17 °C and the mixed chain SOPC has been reported at 6 °C.[69] DPPC has a Tm of 41 °C whereas the fully unsaturated Di-16 : 1-PC has −36 °C[70] suggesting a Tm for the mixed chain lipid just above 0 °C.

The PC system is anticipated to be more fluid and packing defects between saturated and unsaturated species are likely facilitating the insertion of SPs. The PC system enters the LE phase at a molecular area of 110 Å$^2$ mol$^{-1}$ (Fig. 2A). DPPC, the major component at 74%, is responsible for plateau region representing phase coexistence. In the presence of the unsaturated lipids it occurs later at 13 mN m$^{-1}$. This PC mixture collapsed at 42 ± 0.1 mN m$^{-1}$ (Fig. 2A). SP-B$_{1-25}$ peptide increased the lift off area from 110 Å$^2$ mol$^{-1}$ to 120 Å$^2$ mol$^{-1}$ compared, maintained the coexistence phase region at 13 mN m$^{-1}$ and induced film collapse at 44 mN m$^{-1}$. The peptide induced molecular area increase is consistent with the results in Fig. 1 and literature reports.[39,62,65]

PLGA nanoparticles at a 10 : 1 ratio in the subphase caused an earlier lift off by about 8 Å$^2$ mol$^{-1}$, which indicates their interaction with the headgroups (Fig. 2A). The isotherm showed a gentle pressure increase upon compression, characteristic for the LE phase, and the collapse pressure remained at
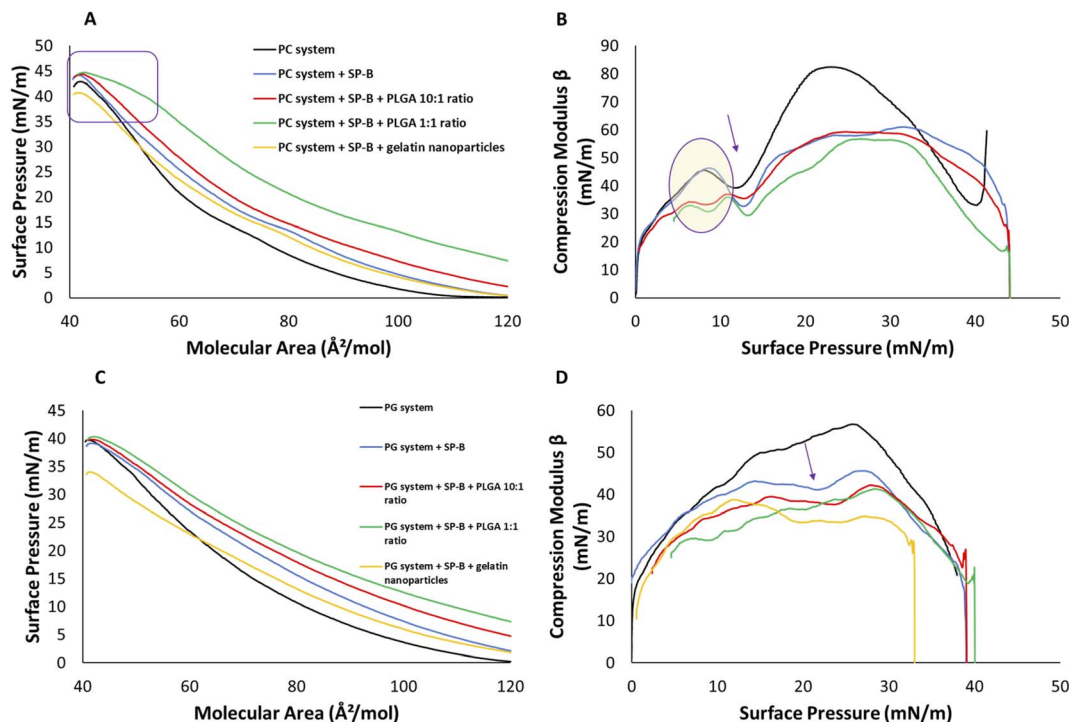
**Fig. 2** Pressure–area isotherms and compression moduli of phosphatidylcholine (PC) and phosphatidylglycerol (PG) containing systems on an aqueous subphase. (A) The pressure–area isotherm of PC system, (B) compression moduli of PC system, (C) the pressure–area isotherm of PG system, and (D) compression moduli of PG system. All systems show results for lipid controls (black), presence of lipid system and SP-B$_{1-25}$ at 10% wt ratio (blue), presence of PLGA at 10 : 1 wt ratio and SP-B$_{1-25}$ at 10% wt ratio (red), presence of PLGA at 1 : 1 wt ratio and SP-B$_{1-25}$ at 10% wt ratio (green), and presence of gelatin NPs at 10 : 1 ratio and SP-B$_{1-25}$ at 10% wt ratio (yellow). The collapse pressures for the isotherms are highlighted (purple box), while dip corresponding to coexistence phase (arrow) and peak modulus (purple oval) are indicated in the compression moduli. All isotherms collected are average of various replicates ($n \geq 3$).

44 mN m$^{-1}$. The addition of particles to the subphase does not provide a quantitative measure of their concentration at the monofilm and considering the much higher subphase volume compared to surface area, the PLGA concentration was also increased to 1 : 1, drastically increasing their impact. At the starting area of ~130 mN m$^{-1}$ the surface pressure was already around 5 mN m$^{-1}$ (Fig. 2A). The isotherm exhibited an overall gentle LE phase slope with a minor discontinuity at 15 mN m$^{-1}$ a pressure range reported for SP-B.[51] The slope change at around 40 mN m$^{-1}$ to a less steep slope suggested the onset of multilayer formation until the same collapse pressure of 44 mN m$^{-1}$ was reached.

GNPs did not affect the lift off area of SP-B$_{1-25}$ system at 120 Å$^2$ mol$^{-1}$ (Fig. 2A). However, upon compression, the isotherm shifted to smaller molecular areas with a reduced shoulder at 15 mN m$^{-1}$ and a reduced collapse pressure of 40 mN m$^{-1}$ indicating a destabilizing effect.

The Cm of the PC system displayed a dip corresponding to coexistence phase at 13 mN m$^{-1}$ (Fig. 2B) and a peak modulus of around 82 mN m$^{-1}$, which was much lower than DPPC alone and is due to increased fluidity of the unsaturated lipids. All other systems showed the isotherm phase coexistence shoulder as isotherm dips between 8 and 15 mN m$^{-1}$ and were more fluid in nature with a maximum Cm of 56 mN m$^{-1}$ compared to 82 mN m$^{-1}$ (Fig. 2B). All systems were similar between 25 and 35

mN m$^{-1}$ with lower Cm values for NP containing films above this range.

The PG system contains DPPG : POPG : SOPG:16 : 0/16-1PG at 1 : 6 : 4.4 : 2 mol ratios which is derived from a mass spectroscopy study.[33] POPG is also very fluid with a Tm of −2 °C.[67] A Tm for SOPG has not been published but PC and PG lipids have similar transition temperatures[71] and the Tm of SOPC has been reported as 6 °C.[69] For the 16 : 0/16 : 1PG (16 : 1PG), a similar Tm as the PC variant can be estimated, which makes the system controlled by fluid lipids.

The area–pressure isotherms in Fig. 2C were more complex than our previously investigated DPPG/POPG. The PG lipid films entered the LE phase at 120 Å$^2$ mol$^{-1}$ and collapsed at a surface pressure of 40 mN m$^{-1}$ (Fig. 2C). The change at 35 mN m$^{-1}$ to a gentler slope could also be due to functional multilayer formation as discussed above. SP-B$_{1-25}$ shifts the transition to the LE phase 12 Å$^2$ mol$^{-1}$ higher than control to 132 Å$^2$ mol$^{-1}$. The slope was gentler with a minor shoulder at 22 mN m$^{-1}$ and a similar collapse pressure of 40 mN m$^{-1}$. The addition of 10 : 1 PLGA NPs increased the molecular area, and the surface pressure to around 3 mN m$^{-1}$ at the starting area of 130 Å$^2$ mol$^{-1}$. The 1 : 1 addition of PLGA nanoparticles isotherm resulted in a starting pressure of 8 mN m$^{-1}$. Both additions did not change the collapse pressure of 40 mN m$^{-1}$ (Fig. 2C). The GNP containing system had the same lift off at 132 Å$^2$ mol$^{-1}$ as

the peptide containing films. However, gelatin NPs resulted in a more gradual increase in surface pressure, a shoulder at 20 mN m$^{-1}$ and earlier collapse than all other systems at 33 mN m$^{-1}$ (Fig. 2C).

The compression modulus profiles displayed a peak of 57 mN m$^{-1}$ at a surface pressure of 26 mN m$^{-1}$ as expected for a system enriched in unsaturated lipids (Fig. 2D). SP-B$_{1-25}$ induced a dip at 22 mN m$^{-1}$, reflecting the shoulder in the area–pressure isotherm, and reached a lower peak value of 46 mN m$^{-1}$ indicating increased fluidity (Fig. 2D, arrow). NP additions only slightly lowered compression modulus values, especially above surface pressures of 30 mN m$^{-1}$, with 35 mN m$^{-1}$ for the PLGA NPs and around 28 mN m$^{-1}$ for GNP which exhibited a maximum of 35 mN m$^{-1}$ at lower pressures (Fig. 2D).

Like for both DPPC and DPPG lipid systems, SP-B$_{1-25}$ increased the molecular area in both PC and PG lipid systems indicating peptide–lipid interactions. The peptide did not affect the stability of PC and PG systems as the collapse pressure was increased for PC by about 2 mN m$^{-1}$ and maintained for the PG system.

Gelatin NPs had stronger interactions, although it must be stated that they are added to the organic phase and may be present in higher concentrations. As previously reported, the addition of GNPs decreased the collapse pressure of the single lipids (PG > PC), and similarly to PC and PG systems reported here (PG > PC, 7 mN m$^{-1}$ vs. 2 mN m$^{-1}$). We have previously observed preferential interaction of GNPs with PG lipids due to electrostatic interaction between positively charged GNPs and negatively charged PGs.[32]

The last system analyzed was the 8 lipid system which contained DPPC : POPC : DPPG : POPG : SOPG : 16-1PC : 16-1PG at 45 : 8 : 1 : 6 : 4.4 : 8 : 2 mol ratio and 2% by weight cholesterol based on previous reports.[33–36] This is the most complex system studied which contains the major PC and PG lipids found in the human lung surfactant along with cholesterol. According to our knowledge, this system has not been studied before as a synthetic biomimetic model. Cholesterol is

a comparably minor component but is essential for proper lung function like low surface tension,[60] and multilayer formation.[25] Its content is maintained between 5 and 10% w/w[11] and higher amounts of the sterol have been linked to acute respiratory distress syndrome.[72]

The 8 lipid system entered the LE phase at 115 Å$^2$ mol$^{-1}$, with a minor shoulder around 15 mN m$^{-1}$ reflecting the pressure range of the potential partial peptide squeeze-out before collapse at a surface pressure of 42 mN m$^{-1}$ (Fig. 4A). SP-B$_{1-25}$ increased the lift off area to 130 Å$^2$ mol$^{-1}$, collapse occurred gradually between 40.8 and 43 mN m$^{-1}$ (Fig. 3A, purple box). The 10 : 1 addition of PLGA NPs had very minor effects below 30 mN m$^{-1}$ but increased the onset of the multilayer formation from 37 to 41 mN m$^{-1}$. The 1 : 1 addition had a starting pressure of 6 mN m$^{-1}$ at 135 Å$^2$ mol$^{-1}$ and larger overall areas suggest enhanced interactions in the headgroup region (Fig. 3A). A wider range of gradual collapse between 38 and 42 mN m$^{-1}$ reflects a slightly reduced stability compared to the 10 : 1 but similar to the lipid and lipid/peptide controls. In contrast to the single lipids and the PC or PG systems, the complex surfactant model was able to withstand the presence of gelatin NPs as the area was only slightly increased with a continuous slope and only a minor reduction of collapse pressure by 2 mN m$^{-1}$ to 40 mN m$^{-1}$ (Fig. 3A).

The Cm data for the 8 lipid system showed a peak rigidity at 86 mN m$^{-1}$ at a surface pressure of 27 mN m$^{-1}$ (Fig. 3B). In the presence of both, SP-B$_{1-25}$ and gelatin NPs, the monolayer elasticity was increased with a peak modulus of around 66 mN m$^{-1}$. Elasticity was further increased in the presence of both SP-B$_{1-25}$ and PLGA NPs at the 1 : 1 ratio with a peak modulus of 57 mN m$^{-1}$. However, PLGA NPs at a 10 : 1 ratio had a much lower elasticity compared to the other NP systems with a peak modulus of 73 mN m$^{-1}$ (Fig. 3B).

However, the major effect of SP-B$_{1-25}$ on collapse can be seen in complex 8 lipid system as the observed multilayer formation allows film compression with less pressure increase compared to controls only containing lipids (Fig. 3A, purple box).[9,16,51,52,73]
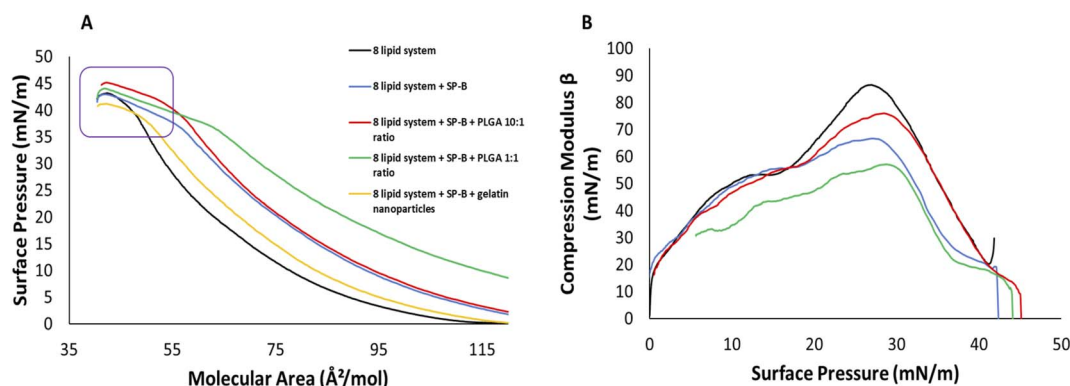


**Fig. 3** Pressure–area isotherms and compression modulus of 8 lipid system on an aqueous subphase. (A) The pressure–area isotherm of 8 lipid system, (B) compression moduli of 8 lipid system. All systems show results for lipid controls (black), presence of lipid system and SP-B$_{1-25}$ at 10% wt ratio (blue), presence of PLGA at 10 : 1 wt ratio and SP-B$_{1-25}$ at 10% wt ratio (red), presence of PLGA at 1 : 1 wt ratio and SP-B$_{1-25}$ at 10% wt ratio (green), and presence of gelatin NPs at 10 : 1 ratio and SP-B$_{1-25}$ at 10% wt ratio (yellow). The collapse pressures for the isotherms are highlighted (purple box). All isotherms collected are average of various replicates ($n \geq 3$).

To a lesser extend this was seen for DPPC as well, the main lipid component of lung surfactant. The squeeze out model[15,66,74–76] suggests that more fluid lipids are removed from the film at lower alveolar areas and concomitant high pressures but SP-B and SP-C help in the folding and formation of surface associated reservoirs during breathing cycles, which mostly consist of unsaturated lipids (Fig. S2†). The remaining saturated lipids at the interface can achieve much lower surface tension values and thus stabilize the surfactant during exhalation potentially in the form of multilayer formation seen here.[9,16,51,52,73] These data confirm the important interplay of lipids and proteins and suggest that the most complex lipid–peptide model system best reflects the currently accepted model of surfactant function.[16]

**3.3.2. Lateral organization.** We have previously applied surface area–pressure isotherms to investigate DPPC[31] or more complex models composed of up to five lipids (DPPC, POPC, DPPG, POPG and Chol) in the absence and presence of gelatin NPs. The results were compared to changes in the lateral film organization visualized by BAM. In all cases, the monolayer results showed moderate increases in surface areas and limited
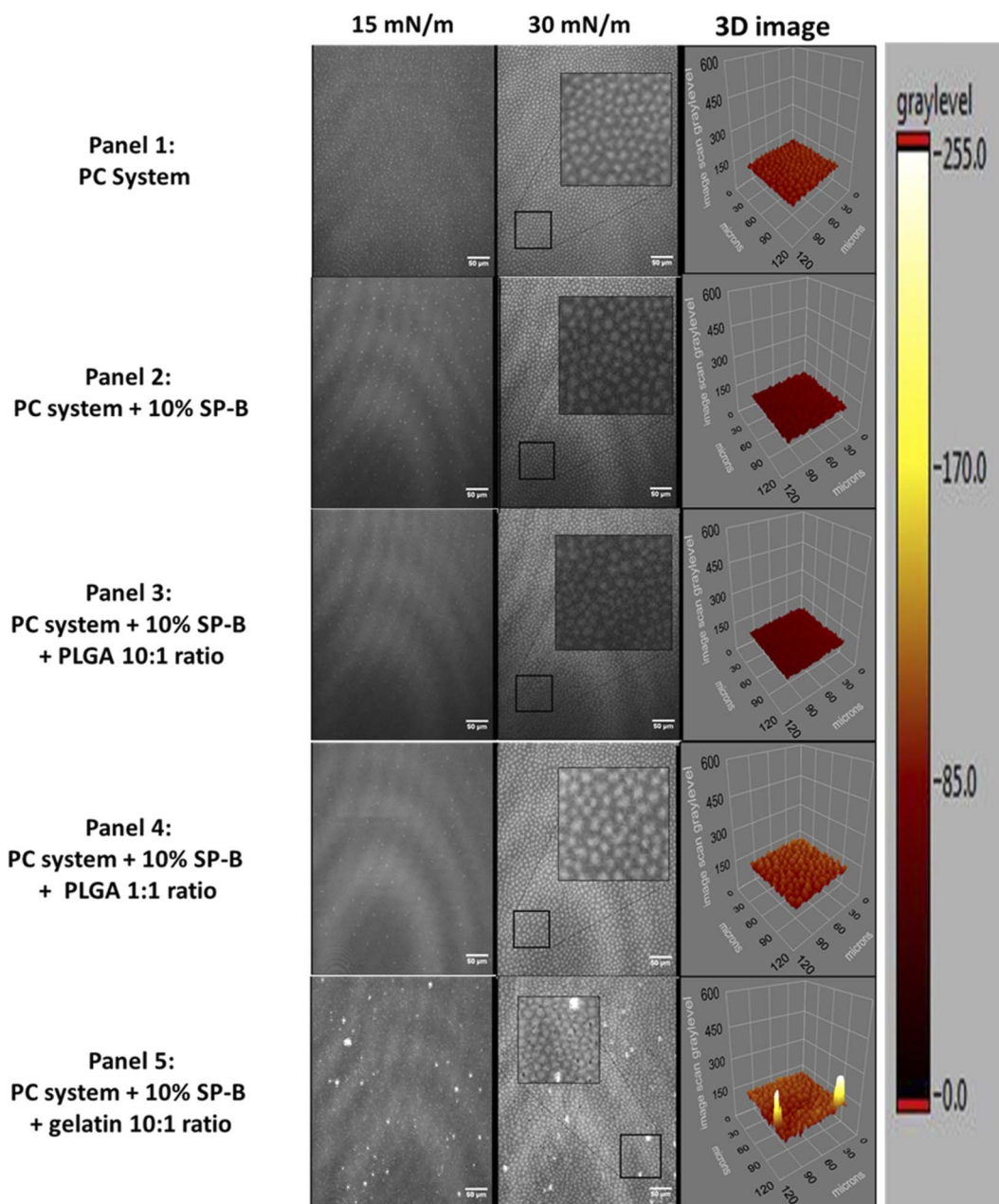


Fig. 4 BAM images of the lateral organization of PC systems on an aqueous subphase at 15 and 30 mN m$^{-1}$ surface pressures. Panel (1) control PC system, panel (2) PC system + 10% SP-B$_{1-25}$, panel (3) PC system + 10% SP-B$_{1-25}$ + PLGA 10 : 1 wt ratio, panel (4) PC system + 10% SP-B$_{1-25}$ + PLGA 1 : 1 wt ratio, and panel (5) PC system + 10% SP-B$_{1-25}$ + gelatin 10 : 1 wt ratio. Scale bar corresponds to 50 µm. Each image is a representation of at least 3 images.

film destabilization, while BAM images illustrated a significant reorganization with less domains.[31] Similar observations were reported using silica nanoparticles[77] and the impact of vaping additives on model lung systems, suggesting that BAM is the more suitable tool for a detailed analysis of the impact of molecules or particles on lung surfactant.[78]

The key forces that determine the domain shape are line tension, favoring rounder domains[79] and electrostatic dipole–dipole repulsion promoting noncircular domains.[80] The single lipids systems have been widely investigated and we present changes induced by the addition of the peptide to DPPC and DPPG in the ESI.† DPPC alone displayed domain formation in the LE/LC phase coexistence region at a surface pressure of around 7 mN m$^{-1}$. Depending on the experimental conditions, bean and tri-loded shapes have been reported.[79,80] In systems including 10% by weight SP-B$_{1-25}$, larger domains were observed that coalesced into a homogenous film earlier than control DPPC (Fig. S4†).
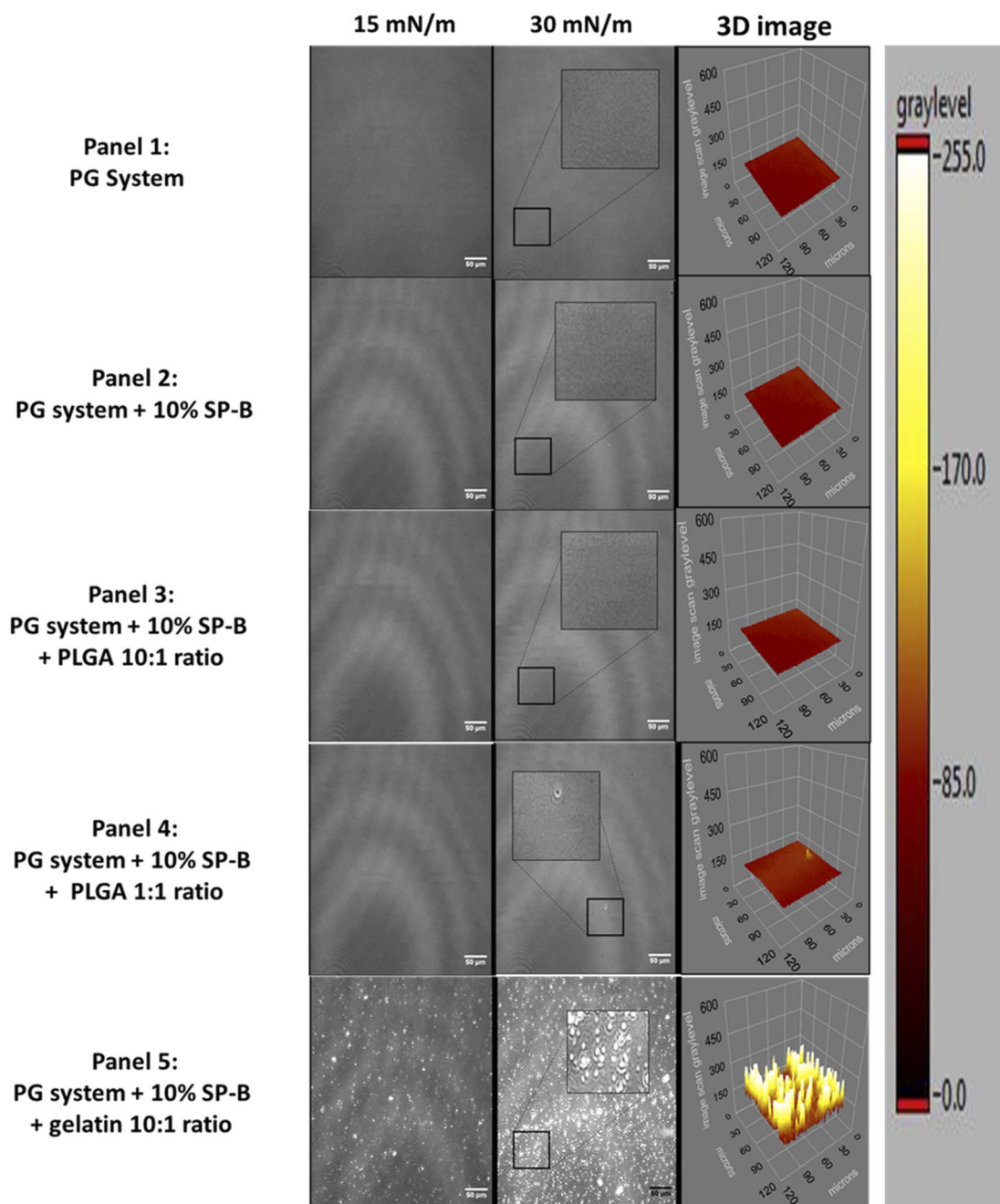


**Fig. 5** BAM images of the lateral organization of PG systems on an aqueous subphase at 15 and 30 mN m$^{-1}$ surface pressures. Panel (1) control PG system, panel (2) PG system + 10% SP-B$_{1-25}$, panel (3) PG system + 10% SP-B$_{1-25}$ + PLGA 10 : 1 wt ratio, panel (4) PG system + 10% SP-B$_{1-25}$ + PLGA 1 : 1 wt ratio, and panel (5) PG system + 10% SP-B$_{1-25}$ + gelatin 10 : 1 wt ratio. Scale bar corresponds to 50 μm. Each image is a representation of at least 3 images.

Control DPPG exhibits almost fully coalesced domains at 15 mN m$^{-1}$ (Fig. S5†). At surface pressures close to 30 mN m$^{-1}$, bright clusters and film defects appeared that remained until monolayer collapse (Fig. S5†). These clusters signify the start of DPPG system collapse which is well documented and reported by other groups.[81,82] The presence of 10% SP-B$_{1-25}$ induced LE/LC phase demixing with numerous lobed domains that exhibit appreciable size variability at around 15 mN m$^{-1}$, domains became smaller and more circular and film coalescence was significantly delayed (Fig. S5†). At increasing pressures, domains started to coalesce but at 30 mN m$^{-1}$, the film was not entirely homogenous yet. Unlike control system, no bright clusters or film defects were seen.

The BAM results indicate that SP-B$_{1-25}$ interacts with DPPC and DPPG differently. With DPPC, the peptide appeared to interact preferentially with the LC form suggested by the increased domain sizes compared to peptide free controls (Fig. S4†). However, for DPPG increased phase demixing and a delay in the formation of a homogenous LC phase was seen in DPPG + SP-B$_{1-25}$ systems (Fig. S5†). A stronger interaction of positively charged SP-B with anionic lipids has been reported.[83] Moreover, the preference of SP-B for the fluid LE phase has been reported as well.[84]

The lateral organization of the PC system is shown in (Fig. 4). The unsaturated POPC and 16 : 0/16 : 1-PC (16-1-PC) reduced and delayed domain formation compared to saturated DPPC. Much smaller domains are observed at 15 mN m$^{-1}$ (Fig. 4, panel 1) that moderately increased in size and frequency upon compression with very comparable sizes to 30 mN m$^{-1}$ and no coalescence was seen until film collapse. With SP-B$_{1-25}$, small domains of a similar size but significantly reduced frequency were recorded (Fig. 4, panel 2). Domains moderately increased in size at 30 mN m$^{-1}$. With gelatin NPs, phase demixing can be seen at low surface pressures that persisted until monolayer collapse (Fig. 4, panel 3 inserts). Bright clusters associated with

gelatin NPs as seen in both DPPC and DPPG systems were also observed throughout the compression.

However, domains can still be seen at around 15 mN m$^{-1}$ and increased at 30 mN m$^{-1}$ (Fig. 4, panel 3). The inserts in each figure are enlarged (as shown for BAM images at 30 mN m$^{-1}$) to better illustrate the lateral organization. The 3D images are based on these selections and allows better visualization of topology changes such as protrusion from the monofilm.

The control PG system contains about 92.5% fluid lipids and thus no domains were seen in the homogeneous LE film (Fig. 5, panel 1). Similarly, the presence of SP-B$_{1-25}$ did not result in any observable changes to the lateral organization (Fig. 5, panel 2). The addition of PGLA only showed minor domain formation at the 1 : 1 ratio. However, the addition of GNPs induced bright clusters throughout the compression that increase in size and numbers, especially noticeable at 30 mN m$^{-1}$ (Fig. 5, panel 3).

This is in agreement with previous results which show reduction in LC domain sizes of DPPC/DPPG mixtures in the presence of SP-B.[84]

A comparison between PC and PG systems is also presented in terms of total area covered by domains in Fig. 6, which shows a progressive reduction for the 10 : 1 (−17%) to the 1 : 1 (−22%). This is consistent with previous work[31] that reported NP induced loss of lateral organization. These rigid domains are important as the anchor regions for hydrophobic SPs, and their disappearance could affect film folding and respreading during the breathing cycle. The more fluid PG system only showed domains with GNP, which are smaller and less frequent compared to GNP in the PC system.

One anomaly was PC system + 10% SPB + 10 : 1 PLGA with a higher domain coverage and frequency than the higher mol ratio of PLGA (Fig. 6).

The lateral organization of the most complex biomimetic system is shown in Fig. 7. Lipid controls exhibited homogenous LE films until monolayer collapse (Fig. 7, panel 1). SP-B$_{1-25}$ only induced very small intermittent domains that persisted until
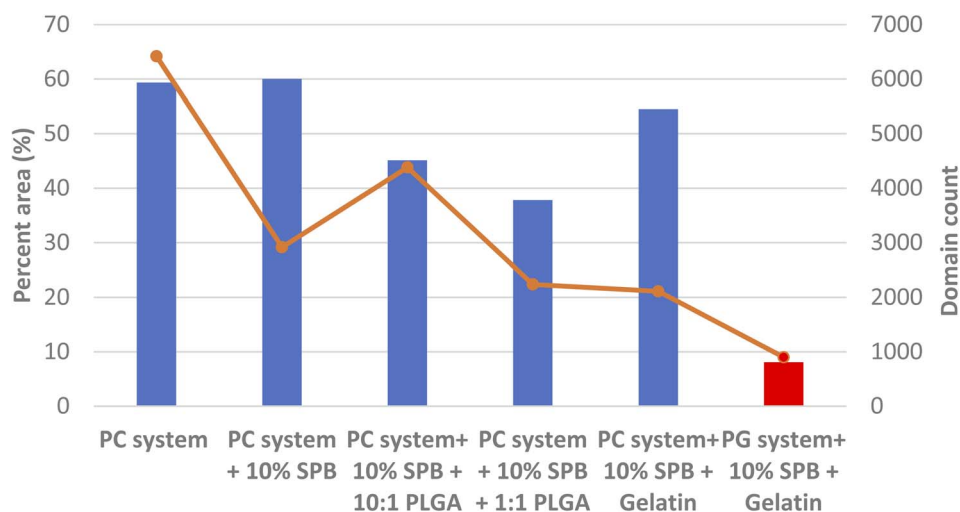


Fig. 6 Quantitative analysis of area percentage (bar) covered by lipid domains and domain frequency (line) on PC and PG systems using representative BAM images at 30 mN m$^{-1}$. This analysis was done using ImageJ software.
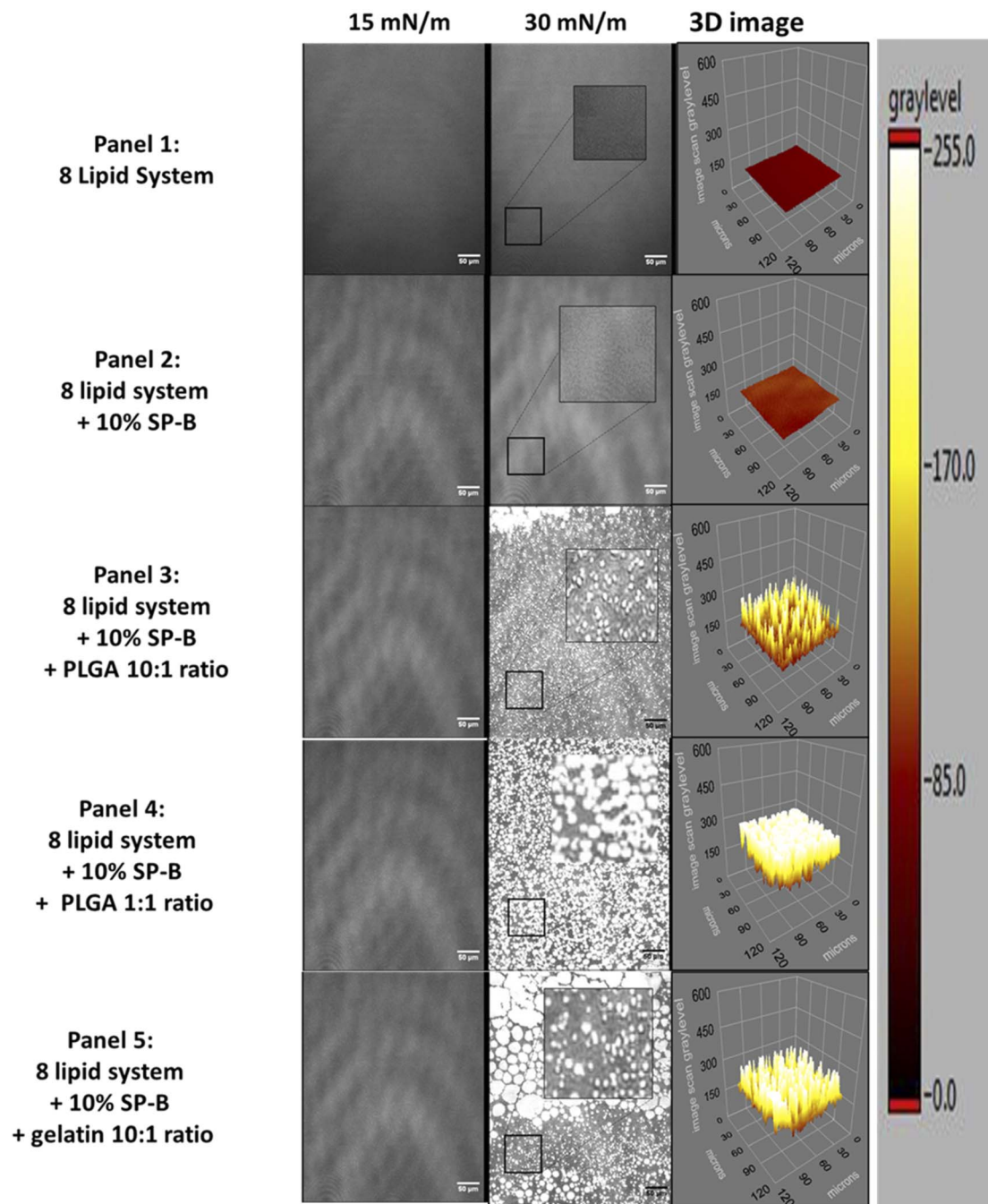
**Fig. 7** BAM images of the lateral organization of 8 lipid systems on an aqueous subphase. Panel (1) control 8 lipid system, panel (2) 8 lipid system in the presence of 10% by weight SP-B$_{1-25}$, panel (3) 8 lipid system in the presence of 10% by weight SP-B$_{1-25}$ and gelatin NPs at a 10 : 1 lipid to NP weight ratio. Panel (4) 8 lipid system + 10% SP-B$_{1-25}$ + PLGA 1 : 1 wt ratio, and panel (5) 8 lipid system + 10% SP-B$_{1-25}$ + gelatin 10 : 1 wt ratio. Scale bar corresponds to 50 μm. Each image is a representative sample ($n \geq 3$).

around 20 mN m$^{-1}$ followed by homogenous film until monolayer collapse (Fig. 7, panel 2). The film organization with GNPs was similar to controls up to pressures closer to 30 mN m$^{-1}$ before numerous bright clusters of varying size, including very large likely coalesced clusters are recorded, indicative of a drastically altered lateral film organization (Fig. 7, panel 3). Unlike previous reports[31] these clusters only appeared after 30 mN m$^{-1}$ but dominated the film structure. The more

complex lipid/peptide system is more able to withstand the impact of NPs.

The complex mixture only shows distinct lateral domains (within the resolution of BAM imaging of 1 μm[85]) in the presence of nanomaterials. The different materials and concentrations have comparable effects in terms of overall domain area but GNP results in larger batches, again possible due to higher concentration within the film, nevertheless, the more
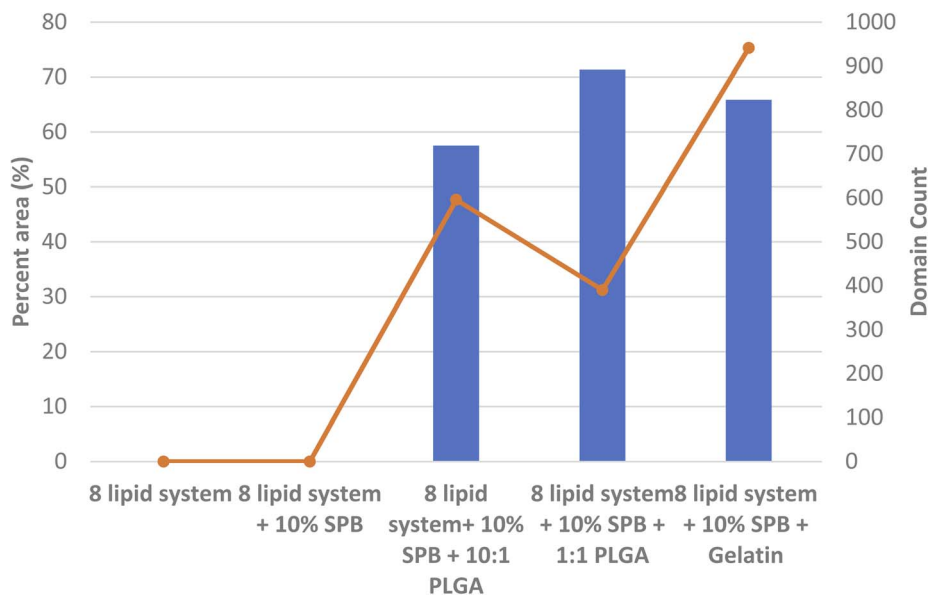
**Fig. 8** Quantitative analysis of area percentage (bar) covered by lipid domains and domain frequency (line) on 8 lipid system using representative BAM images at 30 mN m$^{-1}$. This analysis was done using ImageJ software.

heterogeneous film resulted in a higher overall domain frequency count (Fig. 8B).

Interestingly, we have observed similar 3D protrusion in biomimetic tear film models, where the polar lipid fractions is also enriched in rigid lipids such as DPPC, DPPE, ceramide and sphingomyelin. DPPC was among the lipids that showed indications for reversible multilayer formation, well below the actual film collapse.[86] Indeed, analysis after cycling of these tear film models suggested that the reversible formation and reintegration of 3D protrusions could be important to prevent collapse during blinking.[86]

Positively charged SP-B and its 1–25 peptide has been shown to preferentially interact with anionic phospholipids.[59] MD simulations highlighted the importance of PG lipids and cholesterol for SP–B interaction with lung surfactant. This was further supported by FRET studies supporting the preference for anionic lipids.[87]

As mentioned before, the hydrophobic SPs are important to facilitate reversible film folding during exhalation (squeeze-out), suggesting that they are, at least partially, anchored in LC lipids. DPPC is the main candidate for these interactions, and the observed significant decrease in domain size at 30 mN m$^{-1}$ (Fig. S4†) suggests peptide interactions at the edge of LC domains that limit further size increases. The helical nature of these peptides[56,88] could also promote the formation of helix bundles to further stabilize these structures. Similarly, smaller domains in the presence of 5% SP-B were reported for Survanta, which is a clinically derived bovine lung surfactant[84] SP-B$_{1-25}$ increased the line tension between the LE and LC phases of the PC system, which is energetically unfavorable, leading to smaller LC domain sizes.[84]

The presence of biocompatible gelatin NPs had a significant negative effect on the stability and integrity of three complex model system with the most prominent effects seen in the 8

lipid system. The bright lipid-NP clusters indicate negative effects of these biodegradable and biocompatible NPs that were thought to be safe.

## 4. Conclusion

A highly complex, biomimetic lung surfactant model was developed composed of the major lipids of saturated and unsaturated PCs and PGs and 2% (w/w) of the neutral lipid cholesterol. Furthermore, SP-B$_{1-25}$ was added to assess its interaction with the major lipids of the lung surfactant and NPs.

One of the major goals of our group is the development of a well-defined and representative model of the human lung surfactant to allow for fast initial *in vitro* evaluation of potential NP toxicology through the pulmonary route.

The interaction of SP-B$_{1-25}$ with PC and PG lipids depended on the system. With saturated DPPC, we saw interaction with the LC phase in the form of larger LC domains. When unsaturated PC lipids were present, like in PC system, the interaction appeared to favour the LE phase. However, in both systems, we see an overall fluidization effect after a surface pressure of around 10 mN m$^{-1}$ determined by compression moduli.

For negatively charged PG, interactions were mostly with the LE phase. Like for PC lipids, the peptide caused significant fluidization of PG lipids. As is expected due to positive charge at the NH$_2$-terminal, a stronger effect in terms of significantly reduced collapse pressures was observed for PG systems.

The formation of functional multilayers as suggested here and reported in the literature is important and was shown to prevent premature buckling.[89] These authors suggested that increased film stiffness could negatively affect the monolayer–multilayer conversion. The interaction of nanomaterials, which are much larger than the lipids, will likely reduce local fluidity

and add another negative consequence on top of the induced changes in lateral organization.

We have previously studied GNPs and reported a negative effect on the lateral organization and stability of a simpler 5 lipid model system. These results were confirmed in the more complex system presented here. The elasticity as well as the lateral organization were significantly altered by NPs in all systems analyzed, including the most complex 8 lipid/peptide system.

The appearance of lipid-NP clusters at surface pressures below the monolayer–multilayer transition of lung surfactant indicates that key factors consider for NP drug delivery design such as the material's biodegradability, biocompatibility, and particle size limit[49,90–93] are not sufficient to assess the safety of the drug delivery application as shown here for materials considered as safe.

This ultimately indicates the benefits of having a cheaper, easily assembled and at the same time representative *in vitro* model for initial screening on NP toxicity. This concept was previously shown using polysorbate 80 coated NPs and DPPC models where a drastic decrease in collapse pressure corresponded to acute pulmonary toxicity in mice.[94] As advances in nanomedicine continue to grow, more formulations will need to be evaluated for their potential to impair lung surfactant function. Ultimately, a broader bases screening would allow for correlation between *in vitro* and *in vivo* models[95] which can be used to quickly verify potential toxicity of nanoparticles.

## Abbreviations

| NP | Nanoparticle |
|---|---|
| LE | Liquid expanded |
| LC | Liquid condensed |
| BAM | Brewster angle microscopy |
| SP | Surfactant proteins |
| DPPC | Dipalmitoyl phosphatidylcholine |
| POPC | Palmitoyloleoyl phosphatidylcholine |
| 16-1PC | Palmitoylpalmitoleoyl phosphatidylcholine |
| DPPG | Dipalmitoyl phosphatidylglycerol |
| POPG | Palmitoyloleoyl phosphatidylglycerol |
| SOPG | Stearoyloleoyl phosphatidylglycerol |
| 16-1PG | Palmitoylpalmitoleoyl phosphatidylglycerol |
| Cm | Compressibility |

## Author contributions

WD conducted the experimental work. WD and EJP were involved in experimental planning. PL and KS contributed to data analysis. WD, KS, PL, and EJP contributed to the writing of the final manuscript.

## Conflicts of interest

The authors declare that they have no conflicts of interest with the contents of this article.

## References

1 R. K. Harishchandra, M. Saleem and H. J. Galla, *J. R. Soc., Interface*, 2010, **7**(1), S15–S26.
2 J. Kreuter, *Int. J. Pharm.*, 2007, **331**, 1–10.
3 K. Strebhardt and A. Ullrich, *Nat. Rev. Cancer*, 2008, **8**, 473–480.
4 R. Singh and J. W. Lillard, *Exp. Mol. Pathol.*, 2009, **86**, 215–223.
5 W. H. De Jong and P. J. A. Borm, *Int. J. Nanomed.*, 2008, **3**, 133–149.
6 E. Rytting, J. Nguyen, X. Wang and T. Kissel, *Expert Opin. Drug Deliv.*, 2008, **5**, 629–639.
7 E. R. Weibel, *Physiol. Rev.*, 1973, **53**, 419–495.
8 J. C. Sung, B. L. Pulliam and D. A. Edwards, *Trends Biotechnol.*, 2007, **25**, 563–570.
9 G. Scheuch, M. J. Kohlhaeufl, P. Brand and R. Siekmeier, *Adv. Drug Deliv. Rev.*, 2006, **58**, 996–1008.
10 A. Steimer, E. Haltner and C. M. Lehr, *J. Aerosol Med.*, 2005, **18**, 137–182.
11 T. Hussell and T. J. Bell, *Nat. Rev. Immunol.*, 2014, **14**, 81–93.
12 E. R. Weibel, *Clin. Respir. Physiol.*, 1979, **15**, 999–1013.
13 M. Paranjpe and C. Müller-Goymann, *Int. J. Mol. Sci.*, 2014, **15**, 5852–5873.
14 M. M. Bailey and C. J. Berkland, *Med. Res. Rev.*, 2009, **29**, 196–212.
15 S. Schurch, J. Goerke and J. A. Clements, *Proc. Natl. Acad. Sci. U. S. A.*, 1976, **73**, 4698–4702.
16 R. Veldhuizen, K. Nag, S. Orgeig and F. Possmayer, *Biochim. Biophys. Acta, Mol. Basis Dis.*, 1998, **1408**, 90–108.
17 L. A. J. M. Creuwels, L. M. G. Van Golde and H. P. Haagsman, *Lung*, 1997, **175**, 1–39.
18 M. Agassandian and R. K. Mallampalli, *Biochim. Biophys. Acta, Mol. Cell Biol. Lipids*, 2013, **1831**, 612–625.
19 D. Salgado, R. Fischer, S. Schillberg, R. M. Twyman and S. Rasche, *Front. Immunol.*, 2014, **5**, 623.
20 E. Lopez-Rodriguez and J. Pérez-Gil, *Biochim. Biophys. Acta, Biomembr.*, 2014, **1838**, 1568–1585.
21 R. L. Biltonen and D. Lichtenberg, *Chem. Phys. Lipids*, 1993, **64**, 129–142.
22 M. Hallman, B. H. Feldman, E. Kirkpatrick and L. Gluck, *Pediatr. Res.*, 1977, **11**, 714–720.
23 C. Schleh and J. M. Hohlfeld, *Inhalation Toxicol.*, 2009, **21**, 97–103.
24 J. Pérez-Gil, J. Tucker, G. Simatos and K. M. Keough, *Biochem. Cell Biol.*, 1992, **70**, 332–338.
25 S. Schurch, D. Schurch, T. Curstedt and B. Robertson, *J. Appl. Physiol.*, 1994, **77**, 974–986.
26 J. Perez-Gil and T. E. Weaver, *Physiology*, 2010, **25**, 132–141.
27 J. R. Wright, *Nat. Rev. Immunol.*, 2005, **5**, 58–68.
28 E. Crouch and J. R. Wright, *Annu. Rev. Physiol.*, 2001, **63**, 521–554.

29  S. Orgeig, P. S. Hiemstra, E. J. A. Veldhuizen, C. Casals, H. W. Clark, A. Haczku, L. Knudsen and F. Possmayer, *Respir. Physiol. Neurobiol.*, 2010, **173**, S43–S54.

30  M. Dipasquale, O. Gbadamosi, M. H. L. Nguyen, S. R. Castillo, B. W. Rickeard, E. G. Kelley, M. Nagao and D. Marquardt, *Chem. Res. Toxicol.*, 2020, **33**, 2432–2440.

31  P. Lai, S. Nathoo, T. Ku, S. Gill, S. Azarmi, W. Roa, R. Löbenberg and E. J. Prenner, *J. Biomed. Nanotechnol.*, 2010, **6**, 145–152.

32  W. Daear, P. Lai, M. Anikovskiy and E. J. Prenner, *J. Phys. Chem. B*, 2015, **119**, 5356–5366.

33  A. D. Postle, E. L. Heeley and D. C. Wilton, in *Comparative Biochemistry and Physiology – A Molecular and Integrative Physiology*, Elsevier Inc., 2001, vol. 129, pp. 65–73.

34  M. Amrein, A. Von Nahmen and M. Sieber, *Eur. Biophys. J.*, 1997, **26**, 349–357.

35  A. Kramer, A. Wintergalen, M. Sieber, H. J. Galla, M. Amrein and R. Guckenberger, *Biophys. J.*, 2000, **78**, 458–465.

36  W. Bernhard, H. P. Haagsman, T. Tschernig, C. F. Poets, A. D. Postle, M. E. Van Eijk and H. Von Der Hardt, *Am. J. Respir. Cell Mol. Biol.*, 1997, **17**, 41–50.

37  L. M. Nogee, G. Garnier, H. C. Dietz, L. Singer, A. M. Murphy, D. E. DeMello and H. R. Colten, *J. Clin. Invest.*, 1994, **93**, 1860–1863.

38  J. C. Clark, S. E. Wert, C. J. Bachurski, M. T. Stahlman, B. R. Stripp, T. E. Weaver and J. A. Whitsett, *Proc. Natl. Acad. Sci. U. S. A.*, 1995, **92**, 7794–7798.

39  F. Bringezu, J. Ding, G. Brezesinski, A. J. Waring and J. A. Zasadzinski, *Langmuir*, 2002, **18**, 2319–2325.

40  M. M. Lipp, K. Y. C. Lee, J. A. Zasadzinski and A. J. Waring, *Science*, 1996, **273**, 1196–1199.

41  P. Lai, W. Daear, R. Löbenberg and E. J. Prenner, *Colloids Surf., B*, 2014, **118**, 154–163.

42  E. Locatelli and M. C. Franchini, *J. Nanoparticle Res.*, 2012, **14**, 1–17.

43  F. Danhier, E. Ansorena, J. M. Silva, R. Coco, A. Le Breton and V. Préat, *J. Control. Release*, 2012, **161**, 505–522.

44  J. M. Anderson and M. S. Shive, *Adv. Drug Deliv. Rev.*, 1997, **28**, 5–24.

45  D. Abrams, Y. Huang, S. McQuarrie, W. Roa, H. Chen, R. Löbenberg, S. Azarmi, G. G. Miller and W. H. Finlay, *J. Pharm. Pharm. Sci.*, 2006, **9**(1), 124–132.

46  K. S. Birdi, in *Lipid and Biopolymer Monolayers at Liquid Interfaces*, Springer US, 1989, pp. 57–147.

47  R. E. Brown and H. L. Brockman, *Methods Mol. Biol.*, 2007, **398**, 41–58.

48  M. Broniatowski, M. Flasiński, P. Dynarowicz-Łątka and J. Majewski, *J. Phys. Chem. B*, 2010, **114**, 9474–9484.

49  S. Gill, R. Löbenberg, T. Ku, S. Azarmi, W. Roa and E. J. Prenner, *J. Biomed. Nanotechnol.*, 2007, **3**, 107–119.

50  E. Keating, Y. Y. Zuo, S. M. Tadayyon, N. O. Petersen, F. Possmayer and R. A. W. Veldhuizen, *Biochim. Biophys. Acta, Biomembr.*, 2012, **1818**, 1225–1234.

51  J. Pérez-Gil, *Biochim. Biophys. Acta, Biomembr.*, 2008, **1778**, 1676–1695.

52  J. Ding, D. Y. Takamoto, A. Von Nahmen, M. M. Lipp, K. Y. C. Lee, A. J. Waring and J. A. Zasadzinski, *Biophys. J.*, 2001, **80**, 2262–2272.

53  T. Gröger, S. Nathoo, T. Ku, C. Sikora, R. J. Turner and E. J. Prenner, *Chem. Phys. Lipids*, 2012, **165**, 216–224.

54  G. D. Fidelio, B. Maggio and F. A. Cumar, *Biochem. J.*, 1982, **203**, 717–725.

55  D. Y. Takamoto, M. M. Lipp, A. Von Nahmen, K. Y. C. Lee, A. J. Waring and J. A. Zasadzinski, *Biophys. J.*, 2001, **81**, 153–169.

56  J. Pérez-Gil, C. Casals and D. Marsh, *Biochemistry*, 1995, **34**, 3964–3971.

57  M. L. Longo, A. M. Bisagno, J. A. N. Zasadzinski, R. Bruni and A. J. Waring, *Science*, 1993, **261**, 453–456.

58  K. Nag, S. G. Taneva, J. Perez-Gil, A. Cruz and K. M. W. Keough, *Biophys. J.*, 1997, **72**, 2638–2650.

59  J. Liekkinen, G. Enkavi, M. Javanainen, B. Olmeda, J. Pérez-Gil and I. Vattulainen, *J. Mol. Biol.*, 2020, **432**, 3251–3268.

60  Z. Leonenko, S. Gill, S. Baoukina, L. Monticelli, J. Doehner, L. Gunasekara, F. Felderer, M. Rodenstein, L. M. Eng and M. Amrein, *Biophys. J.*, 2007, **93**, 674–683.

61  S. Taneva and K. M. Keough, *Biophys. J.*, 1994, **66**, 1137–1148.

62  M. A. Oosterlaken-Dijksterhuis, H. P. Haagsman, L. M. G. van Golde and R. A. Demel, *Biochemistry*, 1991, **30**, 10965–10971.

63  S. Schürch, F. H. Y. Green and H. Bachofen, *Biochim. Biophys. Acta, Mol. Basis Dis.*, 1998, **1408**, 180–202.

64  S. L. Duncan and R. G. Larson, *Biochim. Biophys. Acta, Biomembr.*, 2010, **1798**, 1632–1650.

65  S. G. Taneva and K. M. W. Keough, *Biochemistry*, 1994, **33**, 14660–14670.

66  Y. Y. Zuo, R. A. W. Veldhuizen, A. W. Neumann, N. O. Petersen and F. Possmayer, *Biochim. Biophys. Acta, Biomembr.*, 2008, **1778**, 1947–1977.

67  R. Koynova and M. Caffrey, *Biochim. Biophys. Acta, Rev. Biomembr.*, 1998, **1376**, 91–145.

68  A. K. Soutar, H. J. Pownall, A. S. Hu and L. C. Smith, *Biochemistry*, 1974, **13**, 2828–2836.

69  C. Vilchèze, T. P. W. McMullen, R. N. McElhaney and R. Bittmana, *Biochim. Biophys. Acta, Biomembr.*, 1996, **1279**, 235–242.

70  J. R. Silvius and R. N. McElhaney, *Chem. Phys. Lipids*, 1979, **25**, 125–134.

71  J. Li, X. Wang, T. Zhang, C. Wang, Z. Huang, X. Luo and Y. Deng, *Asian J. Pharm. Sci.*, 2015, **10**, 81–98.

72  A. K. Panda, K. Nag, R. R. Harbottle, K. Rodriguez-Capote, R. A. W. Veldhuizen, N. O. Petersen and F. Possmayer, *Am. J. Respir. Cell Mol. Biol.*, 2004, **30**, 641–650.

73  H. Zhang, Y. E. Wang, Q. Fan and Y. Y. Zuo, *Langmuir*, 2011, **27**, 8351–8358.

74  J. Goerke, *Biochim. Biophys. Acta, Mol. Basis Dis.*, 1998, **1408**, 79–89.

75  J. C. Watkins, *Biochim. Biophys. Acta, Lipids Lipid Metab.*, 1968, **152**, 293–306.

76  A. D. Bangham, C. J. Morley and M. C. Phillips, *Biochim. Biophys. Acta, Lipids Lipid Metab.*, 1979, **573**, 552–556.

77 O. Borozenko, M. Faral, S. Behyan, A. Khan, J. Coulombe, C. Dewolf and A. Badia, *ACS Appl. Nano Mater.*, 2018, **1**, 5268–5278.

78 N. van Bavel, P. Lai, R. Loebenberg and E. J. Prenner, *Nanomedicine*, 2022, **17**, 827–843.

79 M. M. Hossain and T. Kato, *Langmuir*, 2000, **16**, 10175–10183.

80 H. M. McConnell and V. T. Moy, *J. Phys. Chem.*, 1988, **92**, 4520–4525.

81 J. Miones, J. M. Rodríguez Patino, O. Conde, C. Carrera and R. Seoane, *Colloids Surf., A*, 2002, **203**, 273–286.

82 R. I. S. Romao, Q. Ferreira, J. Morgado, J. M. G. Martinho and A. M. P. S. G. Da Silva, *Langmuir*, 2010, **26**, 17165–17177.

83 J. Ding, I. Doudevski, H. E. Warriner, T. Alig, J. A. Zasadzinski, A. J. Waring and M. A. Sherman, *Langmuir*, 2003, **19**, 1539–1550.

84 P. Dhar, E. Eck, J. N. Israelachvili, D. W. Lee, Y. Min, A. Ramachandran, A. J. Waring and J. A. Zasadzinski, *Biophys. J.*, 2012, **102**, 56–65.

85 J. Meunier, *Colloids Surf., A*, 2000, **171**, 33–40.

86 M. Patterson, H. J. Vogel and E. J. Prenner, *Biochim. Biophys. Acta, Biomembr.*, 2016, **1858**, 403–414.

87 E. J. Cabré, L. M. S. Loura, A. Fedorov, J. Perez-Gil and M. Prieto, *Biochim. Biophys. Acta, Biomembr.*, 2012, **1818**, 1717–1725.

88 F. Possmayer, S. B. Hall, T. Haller, N. O. Petersen, Y. Y. Zuo, J. Bernardino de la Serna, A. D. Postle, R. A. W. Veldhuizen and S. Orgeig, *Respir. Physiol. Neurobiol.*, 2010, **173**, S55–S64.

89 M. Al-Saiedy, A. Tarokh, S. Nelson, K. Hossini, F. Green, C. C. Ling, E. J. Prenner and M. Amrein, *Biochim. Biophys. Acta, Biomembr.*, 2017, **1859**, 1372–1380.

90 G. Oberdörster, A. Elder and A. Rinderknecht, *J. Nanosci. Nanotechnol.*, 2009, **9**, 4996–5007.

91 E. Guzmán, L. Liggieri, E. Santini, M. Ferrari and F. Ravera, *Colloids Surf., A*, 2012, **413**, 280–287.

92 G. Oberdörster, E. Oberdörster and J. Oberdörster, *Environ. Health Perspect.*, 2005, **113**, 823–839.

93 D. Q. Arick, Y. H. Choi, H. C. Kim and Y. Y. Won, *Adv. Colloid Interface Sci.*, 2015, **225**, 218–228.

94 M. H. D. K. Al-Hallak, S. Azarmi, C. Sun, P. Lai, E. J. Prenner, W. H. Roa and R. Löbenberg, *AAPS J.*, 2010, **12**, 294–299.

95 M. A. Selo, J. A. Sake, K. J. Kim and C. Ehrhardt, *Adv. Drug Delivery Rev.*, 2021, **177**, 113862.